

Two adhesive-contact models for quasistatic mixed-mode delamination problems

CHRISTOS G. PANAGIOTOPOULOS

Institute of Applied and Computational Mathematics, Foundation for Research and Technology - Hellas, Nikolaou Plastira 100, Vassilika Vouton, GR-700 13 Heraklion, Crete, Greece

VLADISLAV MANTIČ

Group of Elasticity and Strength of Materials, Dept. of Continuum Mechanics, School of Engineering, University of Seville, Camino de los Descubrimientos s/n, ES-41092 Sevilla, Spain

TOMÁŠ ROUBÍČEK

Mathematical Institute, Charles University, Sokolovská 83, CZ-186 75 Praha 8, and Institute of Thermomechanics, Czech Academy of Sciences, Dolejškova 5, CZ-182 08 Praha 8, Czech Republic

Abstract. Two models for quasistatic adhesive unilateral contact delaminating in mixed fracture mode, i.e. distinguishing the less-dissipative Mode I (opening) from the more-dissipative Mode II (shearing), and allowing rigorous mathematical and numerical analysis, are studied. One model, referred to as Associative Plasticity-based Rate-Independent Model (APRIM), works for purely elastic bodies and involves, in addition to an interface damage variable, an auxiliary variable (representing interfacial plastic slip) to provide a fracture-mode sensitivity. It relies on a particular concept of force-driven local solutions (given by either vanishing-viscosity concept or maximum-dissipation principle). The other model, referred to as Linear Elastic - (perfectly) Brittle Interface Model (LEBIM), works visco-elastic bodies and rely on a conventional concept of weak solution and needs no auxiliary interfacial variable. This model is directly related to a usual phenomenological model of interface fracture by Hutchinson and Suo used in engineering. This paper devises a way how the phenomenology of the LEBIM can be fit to imitate the APRIM under relatively very slow loading, where both models are essentially rate-independent. The so-called effective dissipated energy is partitioned in both formulations to the surface energy and the energy dissipated during the interface debonding process, where the former is independent and the latter dependent on the fracture mode mixity. A numerical comparison of these models, implemented in a Boundary Element Method (BEM) code, is carried out on a suitable two-dimensional example. Furthermore, the computational efficiency and behaviour of the LEBIM is illustrated on another geometrically more complicated numerical example.

Key Words. Inelastic surface damage, associative rate-independent model, interfacial gradient plasticity with hardening and damage, maximally-dissipative solution, non-associative model, weak solution, semi-implicit discretization, visco-elastic material, quadratic mathematical programming.

AMS Subject Classification: 35K85, 65K15, 65M38, 74M15, 74R20.

1. Introduction – two models

Adhesive contact represents a part of *nonlinear contact mechanics* with numerous practical applications. Modelling damage and fracture of the adhesive layer standardly involves an “internal” variable distributed at the contact surface. Here, this damage-type variable is

denoted by z . This concept, falling in the framework of generalized standard materials [1], was devised by M. Frémond [2, 3].

An important feature appearing in engineering models (and so far mostly omitted in the mathematical literature), is the dependence of this process on the fracture modes under which it proceeds. Indeed, Mode I (=opening) usually dissipates much less energy than Mode II (=shearing). The difference may be up to hundreds of percents, cf. [4, 5, 6, 7, 8]. Moreover, the delamination process seldom occurs in such pure modes and, in reality, the *mixed fracture-mode* appears more frequently. The substantial difference in the dissipation in different modes can be explained either by some roughness of the glued interface (to be overcome in Mode II but not in Mode I, cf. [9]) or by some plastification caused by shear in Mode II (but much less by mere tension in Mode I) before the delamination itself happens, cf. [6, 10]. Let us emphasize that a strong dependence of dissipation (or fracture toughness) on the fracture mode mixity (easily ranging hundreds of percents) has been observed in extensive experiments [4, 9, 5, 6, 8] and thus this phenomenon cannot be neglected in models.

The most common modelling assumption is that the time scale of external load is rather slow so that, in particular the viscous bulk or surface effects are negligible and inelastic processes on the contact surface are much faster so that they are considered rate-independent. Often, also inertial effects are neglected. We also confine ourselves to isothermal models at small strains and frictionless adhesive contact undergoing a unidirectional delamination (i.e. no healing is considered). Most continuum-mechanical models in literature can be (re)formulated as generalized gradient flow or, equivalently as the doubly-nonlinear Biot-type equation:

$$\partial_{\dot{q}}\mathcal{R}(q; \dot{q}) + \partial_q\mathcal{E}(t, q) \ni 0, \quad (1.1)$$

where $q = q(t)$ is a state and \dot{q} denotes its time derivative, \mathcal{R} is a dissipation potential and \mathcal{E} is a stored-energy potential, and “ ∂ ” is a partial generalized derivative (here the convex subdifferential).

Two models developed in the literature that allow for rigorous mathematical and numerical analysis (as far as existence of solutions and numerically stable, implementable, and convergent approximation schemes) are studied here. Both have a bit different character:

LEBIM: *Linear Elastic - (perfectly) Brittle Interface Model* (like [11, 12, 13, 14, 15, 16]):

- + It allows for incorporation of arbitrary *phenomenological* dependence of dissipation (or activation) energy on the fracture mode mixity. The state q in (1.1) is a couple (u, z) and the “elasticity domain” of the adhesive varies depending on the state, which is sometimes called “*non-associative*”, cf. e.g. [17]. Mathematics relies on the conventional concept of weak solution, cf. [18].
- On the other hand, mathematic justification of the merely elastic variant is not available in literature, and a modification by considering a *visco-elastic* rheology of the delaminating bodies seems inevitable, cf. [18]. Thus the viscosity is an additional parameter of the model, which may enrich the modelling aspects but, if the desired model is rather purely elastic, may a bit twist the model.

APRIM: *Associative Plasticity-based Rate-Independent Model* (devised in [19, 20]):

- + Arising from a rational motivation of interfacial *plasticity with hardening*, it uses \mathcal{R} independent of q and degree-1 homogeneous in \dot{q} and works for purely elastic bodies and elasto-plastic adhesive. It involves an auxiliary variable π (called interface plastic slip) to execute the fracture-mode-sensitivity. The state q in (1.1) is a triple (u, z, π) and the “elasticity domain” of the internal variables (z, π) of the adhesive is independent of the state, and such attribute is sometimes denoted by the adjective “associative”.
- It needs a reasonable choice of a solution concept, as discussed for this particular model in [21]. To avoid unwanted effects leading to rather unphysically too early delamination if the energy in the elastic bulk dominates, one must realize a special concept of force-driven local solutions (here either a vanishing-viscosity concept like [22, 23] or solutions complying at least approximately with the maximum-dissipation principle [24, 25, 21]).

It should be emphasized that some other models (mostly representing a variant of the LEBIM or the so-called Cohesive Zone Models (CZM)) are routinely used in engineering even though any rigorous convergence/existence analysis is not at disposal. Such computations and the models themselves are thus unjustified so far from the mathematical point of view, although in particular cases the launched computational simulations may be physically relevant; see e.g. [26, 27, 13, 14, 15, 16] and references therein.

Let us still mention that the LEBIM was rigorously analyzed already in [28] even in a full thermodynamical context but exploiting the concept of non-simple materials (see e.g. [29]) which would be much more demanding to be implemented computationally.

In this paper, after more detailed formulation of the models LEBIM and APRIM in Sections 2 and 3, respectively, we devise a way how the phenomenology of the LEBIM can be fit to imitate the APRIM under very slow loading, where both models are essentially rate-independent and have a good chance to produce similar responses in spite of rather different essence of both models; this is performed in Section 4. Eventually, in Section 5, these models, implemented in a BEM code, are numerically tested and compared on a two-dimensional single-domain example. Furthermore, the solution of a two-domain problem, reproducing the Mixed Mode Flexure (MMF) test, by LEBIM is studied.

Let us first introduce the notation we will use throughout the paper which will be common to both mentioned models. We suppose that the (visco)elastic-bulk/inelastic-adhesive structure occupies a bounded Lipschitz domain $\Omega \subset \mathbb{R}^d$ composed by (for notational simplicity only) two bodies, denoted by Ω_+ and Ω_- , glued together on a common contact boundary, denoted by Γ_C , which represents a prescribed interface where delamination may occur. This means we consider

$$\Omega = \Omega_+ \cup \Gamma_C \cup \Omega_- ,$$

with Ω_+ and Ω_- being disjoint Lipschitz subdomains. We denote by \vec{n} the outward unit normal to $\partial\Omega$, and by \vec{n}_C the unit normal to Γ_C , which we consider oriented from Ω_+ to Ω_- . Moreover, given v defined on $\Omega \setminus \Gamma_C$, v^+ (respectively, v^-) signifies the restriction of v to Ω_+ (to Ω_- , resp.). We further suppose that the boundary of Ω splits as

$$\partial\Omega = \Gamma_D \cup \Gamma_N ,$$

with Γ_D and Γ_N open subsets in the relative topology of $\partial\Omega$, disjoint one from each other, and for $d = 3$ each of them with a smooth (one-dimensional) boundary. Considering $T > 0$

a fixed time horizon, we set

$$Q := (0, T) \times \Omega, \quad \Sigma := (0, T) \times \partial\Omega, \quad \Sigma_C := (0, T) \times \Gamma_C, \quad \Sigma_D := (0, T) \times \Gamma_D, \quad \Sigma_N := (0, T) \times \Gamma_N.$$

For readers' convenience, let us summarize the basic notation used in what follows:

$d = 2, 3$ dimension of the problem,	ψ_G fracture-mode-mixity angle for the LEBIM,
$u : \Omega \setminus \Gamma_C \rightarrow \mathbb{R}^d$ displacement,	$\mathbb{D} \in \mathbb{R}^{d^4}$ viscosity constants for the LEBIM,
$z : \Gamma_C \rightarrow [0, 1]$ delamination variable,	$\alpha = \alpha(\llbracket u \rrbracket)$ effective energy dissipated on Γ_C ,
$e = e(u) = \frac{1}{2} \nabla u^\top + \frac{1}{2} \nabla u$ small-strain tensor,	$w_D : \Sigma_D \rightarrow \mathbb{R}^d$ prescribed boundary displacement,
$\llbracket u \rrbracket = u^- _{\Gamma_C} - u^+ _{\Gamma_C}$ jump of u across Γ_C ,	$f_N : \Sigma_N \rightarrow \mathbb{R}^d$ applied traction,
σ stress tensor,	$\sigma_{t, \text{yield}}$ yield shear stress for the APRIM,
$\mathbb{C} \in \mathbb{R}^{d^4}$ elastic moduli in the Hook law,	$\pi : \Gamma_C \rightarrow \mathbb{R}^{d-1}$ the interfacial plastic slip for APRIM,
$\mathbb{A} \in \mathbb{R}^{d \times d}$ elastic coefficients of the adhesive,	κ_H modulus of kinematic hardening for APRIM,
κ_n distributed normal stiffness,	a_I energy released per unit area in pure Mode I,
κ_t distributed tangential stiffness,	a_{II} energy released per unit area in pure Mode II

Table 1. Summary of the basic notation used throughout the paper.

Throughout the whole paper, we will assume that $\mathbb{C}, \mathbb{D} : \mathbb{R}_{\text{sym}}^{d \times d} \rightarrow \mathbb{R}_{\text{sym}}^{d \times d}$ and $\mathbb{A} : \mathbb{R}^d \rightarrow \mathbb{R}^d$ are linear positive definite, and $\alpha(\cdot) > 0$.

2. The non-associative model (LEBIM)

The *state* is formed by the couple (u, z) . We use *Kelvin-Voigt's rheology* for subdomains (adherents) and, rather for mathematical reasons to facilitate analysis in multidimensional cases, a (possibly only slightly) nonlinear static response. Hence we assume the *stress* $\sigma : Q \rightarrow \mathbb{R}^{d \times d}$ in the form:

$$\sigma = \sigma(u, \dot{u}) := \underbrace{\mathbb{D}e(\dot{u})}_{\text{viscous stress}} + \underbrace{\mathbb{C}e(u)}_{\text{elastic stress}}. \quad (2.1)$$

Furthermore, we shall denote by T_n and T_t the normal and the tangential components of the traction $\sigma|_{\Gamma} \vec{n}$ on some two-dimensional surface Γ (used for either $\Gamma = \Gamma_C$ or $\Gamma = \Gamma_N$), i.e. defined on $\Gamma_C \cup \Gamma_N$ respectively by the formulas

$$T_n = \vec{n} \cdot \sigma|_{\Gamma} \vec{n} \quad \text{and} \quad T_t = \sigma|_{\Gamma} \vec{n} - T_n \vec{n} \quad (2.2)$$

where of course we take as \vec{n} the unit normal \vec{n}_C to Γ_C . Note that T_n is a scalar while T_t is a vector.

The classical formulation of the adhesive contact problem consists, beside the force equilibrium (neglecting body forces) supplemented with standard boundary conditions, from two

complementarity problems on Σ_C . Altogether, we have the boundary-value problem

$$\operatorname{div}(\sigma) = 0, \quad \text{in } Q \setminus \Sigma_C, \quad (2.3a)$$

$$u = w_D \quad \text{on } \Sigma_D, \quad (2.3b)$$

$$\sigma \vec{n} = f_N \quad \text{on } \Sigma_N, \quad (2.3c)$$

$$[[\sigma]] \vec{n}_C = 0 \quad \text{on } \Sigma_C, \quad (2.3d)$$

$$T_t - z(\mathbb{A}[[u]] - (\vec{n}_C \mathbb{A}[[u]]) \cdot \vec{n}_C) = 0 \quad \text{on } \Sigma_C, \quad (2.3e)$$

$$[[u]] \cdot \vec{n}_C \geq 0 \quad \text{and} \quad T_n - z(\mathbb{A}[[u]]) \cdot \vec{n}_C \leq 0 \quad \text{on } \Sigma_C, \quad (2.3f)$$

$$([u] \cdot \vec{n}_C)(T_n - z(\mathbb{A}[[u]]) \cdot \vec{n}_C) = 0 \quad \text{on } \Sigma_C, \quad (2.3g)$$

$$\dot{z} \leq 0 \quad \text{and} \quad \xi \leq \alpha_{\text{PLAST}}([u]) \quad \text{and} \quad \dot{z}(\xi - \alpha_{\text{PLAST}}([u])) = 0 \quad \text{on } \Sigma_C, \quad (2.3h)$$

$$\xi \in \tfrac{1}{2} \mathbb{A}[[u]] \cdot [[u]] - \alpha_{\text{ADHES}} + N_{[0,1]}(z) \quad \text{on } \Sigma_C. \quad (2.3i)$$

In (2.3d), $[[\sigma]]$ denotes naturally the jump of the stress tensor σ across Γ_C so that (2.3d) expresses the equilibrium of tractions on Γ_C . The complementarity problem (2.3f)–(2.3g) describes the frictionless Signorini unilateral contact. The complementarity problem (2.3h)–(2.3i) corresponds to the *flow rule* governing the evolution of z :

$$\tfrac{1}{2} \mathbb{A}[[u]] \cdot [[u]] + N_{(-\infty, 0]}(\dot{z}) + N_{[0, 1]}(z) \ni \alpha_{\text{ADHES}} + \alpha_{\text{PLAST}}([u]) =: \alpha([u]) \quad \text{in } \Sigma_C, \quad (2.4)$$

with $N_{(-\infty, 0]}, N_{[0, 1]} : \mathbb{R} \rightrightarrows \mathbb{R}$ denoting the normal cones (in the sense of convex analysis) to the intervals $(-\infty, 0]$ and $[0, 1]$, respectively. For more details about derivation of the model we refer to [28, 30]. We will consider the initial-value problem for (2.3) by prescribing the initial condition

$$u(0) = u_0 \quad \text{a.e. in } \Omega \quad \text{and} \quad z(0) = z_0 \quad \text{a.e. in } \Gamma_C. \quad (2.5)$$

In the weak formulation, the boundary-value problem (2.3) takes the abstract form (1.1), i.e. now the doubly-nonlinear Biot-type system of two inclusions:

$$\partial_{\dot{u}} \mathcal{R}(\dot{u}) + \partial_u \mathcal{E}(t, u, z) \ni 0 \quad \text{and} \quad \partial_{\dot{z}} \mathcal{R}(u; \dot{z}) + \partial_z \mathcal{E}(u, z) \ni 0, \quad (2.6)$$

provided \mathcal{E} and \mathcal{R} are taken as

$$\mathcal{E}(t, u, z) := \begin{cases} \frac{1}{2} \int_{\Omega \setminus \Gamma_C} \mathbb{C} e(u) : e(u) \, dx - \int_{\Gamma_N} f_N(t) \cdot u \, dS \\ \quad + \frac{1}{2} \int_{\Gamma_C} z \mathbb{A}[[u]] \cdot [[u]] - \alpha_{\text{ADHES}} z \, dS & \text{if } u = w_D(t) \text{ on } \Gamma_D, \\ & [[u]] \cdot \vec{n}_C \geq 0 \text{ and } 0 \leq z \leq 1 \text{ on } \Gamma_C, \\ +\infty & \text{otherwise,} \end{cases} \quad (2.7)$$

and

$$\mathcal{R}(u; \dot{u}, \dot{z}) := \begin{cases} \frac{1}{2} \int_{\Omega \setminus \Gamma_C} \mathbb{D} e(\dot{u}) : e(\dot{u}) \, dx + \int_{\Gamma_C} \alpha_{\text{PLAST}}([u]) |\dot{z}| \, dS & \text{if } \dot{z} \leq 0 \text{ a.e. in } \Gamma_C, \\ +\infty & \text{otherwise.} \end{cases} \quad (2.8)$$

Note that the *effective dissipated energy*

$$\alpha([u]) = \alpha_{\text{ADHES}} + \alpha_{\text{PLAST}}([u]) \quad (2.9)$$

is, in general, composed from a part α_{ADHES} interpreted as an *adhesion energy* stored by creating a new surface by delamination and another part, denoted by α_{PLAST} , interpreted as an *energy dissipated by the plastification* process during delamination. Altogether, $\alpha_{\text{ADHES}} + \alpha_{\text{PLAST}}$ is to be understood as a *fracture energy* (sometimes also referred to as *fracture toughness*). Only the plastification energy is considered as dependent on the delamination mode, and is usually increasing from pure Mode I to pure Mode II, and need not be zero even in pure Mode I, cf. [31, Fig. 4.2], [9, Fig. 1] or [32, Fig. 2]. As the delamination is considered here as a unidirectional process, the part α_{ADHES} cannot be refreshed back and is effectively dissipated, too. Both parts would be distinguished if \mathcal{R} would be finite (i.e. healing or re-bonding of the adhesive would be allowed) or if the full thermodynamical context would be considered (then only α_{PLAST} but not α_{ADHES} would contribute to the heat production).

A standard engineering approach, as e.g. in [5, 13, 14, 15], is that \mathbb{A} is diagonal in a local coordinate system associated to Γ_c , writing e.g. $\mathbb{A} = \text{diag}(\kappa_n, \kappa_t, \kappa_t)$ for $\vec{n}_c = (1, 0, 0)$ at some $x \in \Gamma_c$, and the activation energy denoted here by α , whereas in engineering typically referred to as fracture energy and denoted by G_c , depends on the so-called *energetic fracture-mode-mixity angle* ψ_G defined as

$$\psi_G = \psi_G(\llbracket u \rrbracket) := \arctan \left(\sqrt{\frac{\kappa_t}{\kappa_n}} \frac{|\llbracket u \rrbracket_t|}{|\llbracket u \rrbracket_n|} \right), \quad (2.10)$$

where $\llbracket u \rrbracket_t$ and $\llbracket u \rrbracket_n$ stand for the tangential and the normal relative displacements; i.e. the jump of displacement across the boundary Γ_c decomposes as $\llbracket u \rrbracket = \llbracket u \rrbracket_n \vec{n}_c + \llbracket u \rrbracket_t$, with $\llbracket u \rrbracket_n = \llbracket u \rrbracket \cdot \vec{n}_c$. Occasionally, other fracture-mode-mixity angles may be defined as associated to displacements or stresses, $\psi_u = \arctan(|\llbracket u \rrbracket_t|/|\llbracket u \rrbracket_n|)$ and $\psi_\sigma = \arctan(\kappa_t |\llbracket u \rrbracket_t| / \kappa_n |\llbracket u \rrbracket_n|)$, respectively. Here, we will not use any of the phenomenological laws for $G_c(\psi_G)$ well-known in engineering (see [13]) but rather fit it with the plasticity-inspired model described in the following section.

3. The associative plasticity-based model (APRIM)

In accordance with other experimental observations and computational models [6, 10, 33], the associated plastic zones in the adjacent bulk, near the crack tip, are larger in Mode II than in Mode I and these plastic phenomena are localized in a relatively narrow plastic zone in the bulk in the interface vicinity. In order to provide a better representation of these experimental results, a plastic tangential response has been assumed at the interface, which allows us to distinguish between fracture Mode I and II in the sense that some additional dissipated energy is associated to interface fracture in Mode II. In our works [19, 20, 34], imitating the conventional models of linearized single-threshold plasticity with kinematic hardening (e.g. [17]), we have invented a plastic slip variable π as another internal variable on the delaminating surface (in addition to z) whose evolution activates in Mode II but not in Mode I in order to achieve the desired mixity-mode-dependent dissipation. In contrast to the LEBIM from Section 2, the mathematical analysis now needs a gradient theory used for some of the internal variables; here, following [25], we apply it on π rather than on z as in [19, 20].

Instead of (2.1), we consider purely elastic material now:

$$\sigma = \sigma(u) := \mathbb{C}e(u). \quad (3.1)$$

In the classical formulation, referring to (2.2), this model uses again (2.3a-d) completed now by

$$T_t - z(w - (w \cdot \vec{n}_C)\vec{n}_C) = 0 \quad \text{with } w := \mathbb{A}(\llbracket u \rrbracket - \mathbb{T}\pi) \quad \text{on } \Sigma_C, \quad (3.2a)$$

$$\llbracket u \rrbracket \cdot \vec{n}_C \geq 0 \quad \text{and} \quad T_n - z w \cdot \vec{n}_C \leq 0 \quad \text{and} \quad (\llbracket u \rrbracket \cdot \vec{n}_C)(T_n - z w \cdot \vec{n}_C) = 0 \quad \text{on } \Sigma_C, \quad (3.2b)$$

$$\dot{z} \leq 0 \quad \text{and} \quad \xi \leq a_1 \quad \text{and} \quad \dot{z}(\xi - a_1) = 0 \quad \text{with } \xi \in \frac{1}{2}w \cdot \mathbb{A}^{-1}w - a_0 + N_{[0,1]}(z) \quad \text{on } \Sigma_C, \quad (3.2c)$$

$$\dot{\pi} = \begin{cases} 0 & \text{if } |\zeta| < \sigma_{t,\text{yield}} \\ \lambda \zeta, \quad \lambda \geq 0 & \text{if } |\zeta| = \sigma_{t,\text{yield}}, \end{cases} \quad \text{and} \quad |\zeta| \leq \sigma_{t,\text{yield}} \quad \text{with}$$

$$\zeta = T_n - \text{div}_s(\kappa_G \nabla_s \pi) + (\text{div}_s \vec{n}_C)(\kappa_G \nabla_s \pi \cdot \vec{n}_C) - \kappa_H \pi \quad \text{on } \Sigma_C, \quad (3.2d)$$

where $\mathbb{T} = \mathbb{T}(x) : \mathbb{R}^{d-1} \rightarrow \mathbb{R}^d$ denotes the mapping from the space where π has values to the tangent space of the d -dimensional space where $\llbracket u \rrbracket$ has values. This mapping allows to sum up $(d-1)$ -dimensional vector π with the d -dimensional vector $\llbracket u \rrbracket$, as needed in (3.2a) and later in (3.4a), too. In (3.2d), $\kappa_G > 0$ is a (presumably small) parameter determining length-scale of spatial variation of π . Also note that ξ and ζ denote the available driving forces for the activated evolution of z and π , respectively. In (3.2d), $\text{div}_s := \text{trace}(\nabla_s)$ denotes the $(d-1)$ -dimensional “surface divergence” and ∇_s a “surface gradient”, i.e. the tangential derivative defined as $\nabla_s v = \nabla v - (\nabla v \cdot \vec{n}_C)\vec{n}_C$ for v defined on Γ_C .

In addition to the boundary conditions (2.3b,c), due to the surface gradient of π , we now need also the condition for π . Most naturally, we assume:

$$\nabla_s \pi \cdot \vec{\nu}_C = 0 \quad \text{on } \partial\Gamma_C, \quad (3.2e)$$

where $\vec{\nu}_C$ denotes the unit vector lying in Γ_C and being outward normal to $\partial\Gamma_C$. Of course, the boundary/transmission-value problem (2.3a-d) with (3.1) and (3.2a-e) is to be completed by the initial conditions. Assuming undamaged and unplasticized adhesive at the beginning, we consider

$$\pi(0, \cdot) = \pi_0 = 0 \quad \text{and} \quad z(0, \cdot) = z_0 = 1. \quad (3.2f)$$

Note that we are now choosing a specific z_0 in (2.5) and, in contrast to (2.5), the initial condition for u is now irrelevant or, more precisely, it follows from (3.2f) because $u(0)$ is assumed to solve the boundary/transmission-value problem (2.3a-d) with (3.1) and (3.2a,b). The last term in (3.2d) involves $(\text{div}_s \vec{n}_C)$ which is (up to a factor $-\frac{1}{2}$) the mean curvature of the surface Γ_C , and it arises by applying a Green’s formula on a curved surface

$$\int_{\Gamma_C} \tilde{v} : ((\nabla_s v) \otimes \vec{n}_C) dS = \int_{\Gamma_C} (\text{div}_s \vec{n}_C) (\tilde{v} : (\vec{n}_C \otimes \vec{n}_C)) v - \text{div}_s(\tilde{v} \cdot \vec{n}_C) v dS + \int_{\partial\Gamma_C} (\tilde{v} \cdot \vec{\nu}_C) v dl \quad (3.3)$$

used with $\tilde{v} = \kappa_G \nabla_s \pi$ and with the boundary condition $\tilde{v} \cdot \vec{\nu}_C = 0$ on $\partial\Gamma_C$, cf. (3.2e), for the directional-derivative term $\int_{\Gamma_C} \kappa_G \nabla_s \pi \cdot \nabla_s \tilde{\pi} dS$ arising from the term $\int_{\Gamma_C} \frac{1}{2} \kappa_G |\nabla_s \pi|^2 dS$ in (3.4a). The Green-type identity (3.3) was used in a similar context in mechanics of complex (also called non-simple) continua, cf. [29, 35].

This quite complicated boundary-value problem can still be covered by the simple and elegant Biot’s form (1.1) even with $\mathcal{R}(q, \dot{q})$ independent of q , which is why we used the

adjective “associative”, provided the state $q = (u, z, \pi)$ and provided the stored-energy functional is taken as

$$\mathcal{E}(t, u, z, \pi) := \begin{cases} \int_{\Omega \setminus \Gamma_C} \frac{1}{2} \mathbb{C} e(u) : e(u) \, dx + \int_{\Gamma_C} \left(\frac{1}{2} z \mathbb{A}(\llbracket u \rrbracket - \mathbb{T} \pi) \cdot (\llbracket u \rrbracket - \mathbb{T} \pi) - a_0 z \right. \\ \quad \left. + \frac{\kappa_H}{2} |\pi|^2 + \frac{\kappa_G}{2} |\nabla_s \pi|^2 \right) \, dS - \int_{\Gamma_N} f_N(t) \cdot u \, dS & \text{if } u = w_D(t) \text{ on } \Gamma_D, \\ & 0 \leq z \leq 1 \text{ on } \Gamma_C, \text{ and} \\ & \llbracket u \rrbracket_n \geq 0 \text{ on } \Gamma_C, \\ +\infty & \text{elsewhere,} \end{cases} \quad (3.4a)$$

while the dissipation-energy potential is taken as

$$\mathcal{R}(\dot{z}, \dot{\pi}) := \begin{cases} \int_{\Gamma_C} a_1 |\dot{z}| + \sigma_{t, \text{yield}} |\dot{\pi}| \, dS & \text{if } \dot{z} \leq 0 \text{ a.e. on } \Gamma_C, \\ +\infty & \text{otherwise.} \end{cases} \quad (3.4b)$$

Actually, the doubly-nonlinear Biot-type equation (1.1) can now be written as three inclusions:

$$\partial_u \mathcal{E}(t, u, z, \pi) \ni 0, \quad \partial_{\dot{z}} \mathcal{R}(\dot{z}) + \partial_z \mathcal{E}(u, z, \pi) \ni 0 \quad \text{and} \quad \partial_{\dot{\pi}} \mathcal{R}(\dot{\pi}) + \partial_{\pi} \mathcal{E}(u, z, \pi) \ni 0. \quad (3.5)$$

Similarly as in Section 2, the *effective dissipation energy* in Mode I, denoted here by a_1 , is composed from two parts, namely the *surface energy* a_0 associated to the creation of a new surface and the energy dissipated by debonding process a_1 , i.e.

$$a_1 := a_0 + a_1. \quad (3.6)$$

As in (2.10), we will consider that $\mathbb{A} = \text{diag}(\kappa_n, \kappa_t, \kappa_t)$ in a local coordinate system with $\vec{n}_C = (1, 0, 0)$. Starting from the initial conditions (3.2f), the response in pure Mode I is essentially determined by κ_n and a_1 because pure opening neither triggers the evolution of π nor causes $\llbracket u \rrbracket_t \neq 0$, cf. Fig.1(Left). To analyse the response in pure Mode II, let us realize that the tangential stress σ_t is a derivative of \mathcal{E} with respect to $\llbracket u \rrbracket_t$, and thus $\sigma_t = \sigma_t(u, \pi) = \kappa_t(\llbracket u \rrbracket_t - \pi)$ if $z = 1$. In analogy with the conventional plasticity, the slope of the evolution of π vs. $\llbracket u \rrbracket_t$ under hardening is $\kappa_t/(\kappa_t + \kappa_H)$.

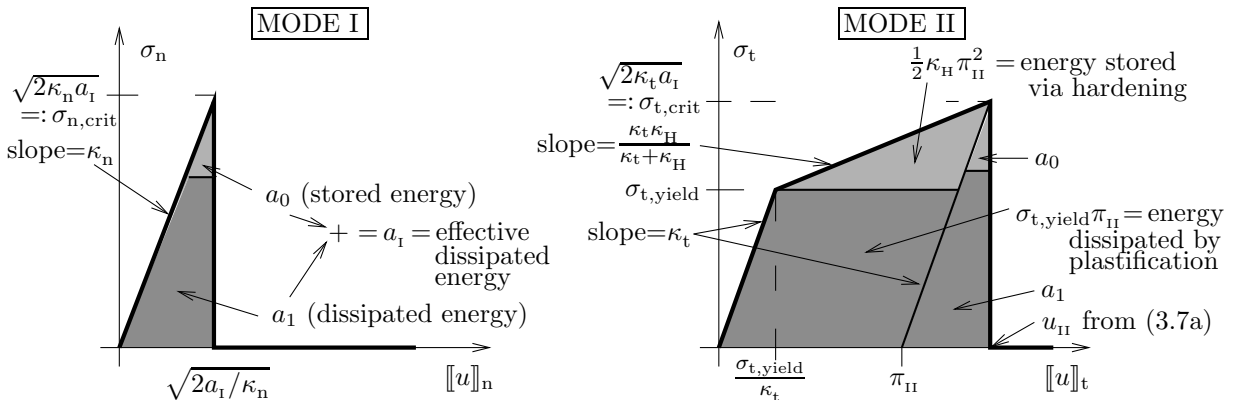


Fig. 1. Schematic illustration of the stress-relative displacement law in the model (3.4) for $d = 2$ and $\mathbb{A} = \text{diag}(\kappa_n, \kappa_t)$ in the opening (Mode I) and the shearing (Mode II) experiments, considering $z_0 = 1$ and $\pi_0 = 0$. The partition of the effective dissipated energy is depicted only formally. The contribution of the delamination-gradient term is neglected, i.e. $\kappa_G = 0$.

From Fig. 1(Right), one can see that delamination in pure Mode II is triggered if $\frac{1}{2}\kappa_t|\llbracket u \rrbracket_t - \pi|^2 = \frac{1}{2}\sigma_t^2/\kappa_t$ attains the threshold a_I , i.e. if the tangential stress σ_t achieves the critical stress $\sigma_{t,\text{crit}} = \sqrt{2\kappa_t a_I}$. Delamination in Mode II is thus triggered by the tangential displacement u_{II} and the tangential slip π_{II} given by

$$u_{II} = \frac{\sqrt{2\kappa_t a_I}(\kappa_t + \kappa_H) - \sigma_{t,\text{yield}}\kappa_t}{\kappa_t \kappa_H} \quad \text{and} \quad \pi_{II} = \frac{\sqrt{2\kappa_t a_I} - \sigma_{t,\text{yield}}}{\kappa_H} \quad (3.7a)$$

and, after some algebra, one can see that the overall *effective dissipation energy* in Mode II, denoted here by a_{II} , is composed from four parts, cf. Fig. 1(Right), namely

$$a_{II} = a_I + \sigma_{t,\text{yield}}\pi_{II} + \frac{1}{2}\kappa_H\pi_{II}^2 = \underbrace{a_1 + \sigma_{t,\text{yield}}\pi_{II}}_{\text{arising from the dissipated energy } \mathcal{R}} + \underbrace{a_0 + \frac{1}{2}\kappa_H\pi_{II}^2}_{\text{arising from the stored energy } \mathcal{E}} \quad (3.7b)$$

provided $2\kappa_t a_I \geq \sigma_{t,\text{yield}}^2$, and taking into account that the evolution of π will stop evolving after delamination is completed. To have actually this behaviour, the parameters should satisfy

$$\frac{1}{2}\sqrt{2\kappa_t a_I} < \sigma_{t,\text{yield}} \leq \sqrt{2\kappa_t a_I}. \quad (3.8)$$

After some algebra, from (3.7) it results that $\kappa_H\pi_{II} = \kappa_t\kappa_H(u_{II} - \sigma_{t,\text{yield}}/\kappa_t)/(\kappa_t + \kappa_H)$, cf. Fig. 1(Right). A measure of maximum *fracture-mode sensitivity* a_{II}/a_I is then indeed bigger than 1, namely

$$\frac{a_{II}}{a_I} = 1 + \left(\sigma_{t,\text{yield}}\pi_{II} + \frac{\kappa_H\pi_{II}^2}{2} \right) / a_I = 1 + \frac{\kappa_t}{\kappa_H} - \frac{\sigma_{t,\text{yield}}^2}{2\kappa_H a_I}. \quad (3.9)$$

Like discussed already for (2.9), also here the particular contributions in the splitting (3.6) could be distinguished only in a full thermodynamical model where a_1 (together possibly with $\sigma_{t,\text{yield}}\pi_{II}$) would contribute to the heat production while a_0 (together possibly with $\frac{1}{2}\kappa_H\pi_{II}^2$) would not, cf. also the splitting (3.7b).

The vital part of the rate-independent models themselves is a suitable choice of a concept of solutions. Let us emphasize that the class of the so-called local (in fact weak [24]) solutions to nonconvex rate-independent systems like this one given by (3.4) is typically very wide and not every type solution will serve well in our context. For example, the so-called energetic solutions [36] which conserves energy will have a tendency for too early rupture preferably in less dissipative mode, i.e. here Mode I. Here, as we want to relate APRIM with LEBIM, we should consider a *force-driven-like local solution*, which is physically relevant and comparable with the conventional weak solution concept for the viscous LEBIM. See [37] for a comparison of various concepts of local solution to rate-independent systems, and [21] for a numerical comparison of the energetic and a particular local solution.

A physically justified concept of local solutions is a *vanishing-viscosity solution*, obtained by considering small viscosity in the bulk like in the LEBIM or/and in the adhesive and pass it to zero. The limit, if exists, is the vanishing-viscosity solution. When combined with a suitable spatial discretisation, a control of the (approximate) energy conservation needs very fine time discretisation for small viscosities, cf. [23], and therefore this method is computationally quite heavy.

Computationally very efficient but physically in general rather ad-hoc method (cf. the discussion in [24]), which however has a guaranteed convergence (in terms of subsequences) towards local solutions devised in [25], is based on a semi-implicit discretisation of the fractional-step type, cf. (5.2) below. Cf. also [38, Sect. 4.3.4.3].

4. Reading information from APRIM to be used in LEBIM

We further proceed by describing the APRIM in terms of the *effective dissipated energy*, also referred to as a *fracture energy* $\alpha(\cdot) = G_c(\cdot)$, for which it can be shown [13, 39, 40, 41, 42] that equals the energy per unit area stored in the adhesive at the crack tip. In principle, one can imagine various strategies fitting LEBIM towards APRIM, justified from the perspective of plastification like suggested in [6, 10] as an explanation of the fracture-mode-mixity sensitivity, or even conversely fitting APRIM towards a given phenomenology of LEBIM.

Here, rather as an example, we will make the fitting of LEBIM to APRIM in such a way that Mode I will be the same for both models while, in Mode II, the overall dissipated energy will be the same for both models, cf. Fig. 2. Two scenarios for fitting their constitutive law of interface are considered. In the first one, the initial stiffness of the adhesive layer is fitted, Fig. 2(Left). In the second one, the relative tangential displacement causing the rupture in Mode II will be equal, then the tangential adhesive stiffness in the matrix \mathbb{A} for LEBIM, namely $\kappa_t = 2a_{\text{II}}/u_{\text{II}}^2$ with a_{II} and u_{II} from (3.7), will be lower than the adhesive stiffness κ_t in APRIM, Fig. 2(Right).

With reference to the first scenario, a certain misfit in the results can be expected because the LEBIM fitted according to Fig. 2(Left) is elastically stiffer in Mode II than APRIM for sufficiently large stresses, whereas the LEBIM fitted according to Fig. 2(Right) is at least initially more compliant. Thus, we can expect that some parts in the resulting global behaviour of both models will be better fitted in one scenario, but expectedly this will create a certain misfit in some other parts.

One should also realize that APRIM has some unexploited freedom: e.g. one can consider a non-linear hardening, i.e. a non-quadratic term instead of $\frac{1}{2}\kappa_{\text{H}}|\pi|^2$ in (3.4a). Having used a gradient term in (3.4a), this generalization would still allow for a mathematical support. Similarly, the elastic \mathbb{A} -term in (3.4a) can be made non-quadratic. Obtaining such a freedom, one can then try conversely to fit APRIM towards LEBIM with a given phenomenological nonlinearity $\alpha(\cdot)$.

In engineering applications, the phenomenological law of G_c proposed in [5], cf. [4, 13], is usually applied,

$$G_c(\psi_G) = a_I(1 + \tan^2((1-\lambda)\psi_G)), \quad (4.1)$$

where $a_I = G_c(0^\circ)$ gives the fracture energy in Mode I, and λ is the so-called mode sensitivity parameter, $0 \leq \lambda \leq 1$. A moderately strong fracture-mode sensitivity occurs when the ratio a_{II}/a_I is about 5-10 (see Fig. 3(a)), with $a_{\text{II}} = G_c(90^\circ)$ the fracture energy in Mode II, which happens for λ about 0.2-0.3. A numerical implementation of (4.1) in the above non-associative model was presented in [18].

In a theoretical study of the behaviour of APRIM, including an interface plastic slip variable, the following functional dependence of $G_c(\psi_G)$ was deduced in [34, 43], while an

in-depth analysis and detailed description was presented in [21],

$$\alpha(\llbracket u \rrbracket) := G_c(\psi_G(\llbracket u \rrbracket))$$

$$= \begin{cases} a_I, & \text{for } 0 \leq \psi_G \leq \arcsin \frac{\sigma_{t,\text{yield}}}{\sqrt{2\kappa_t a_I}}, \\ \frac{2a_I(\kappa_t + \kappa_H) - \sigma_{t,\text{yield}}^2}{2(\kappa_t + \kappa_H + \kappa_H \tan^2 \psi_G)} (1 + \tan^2 \psi_G) & \text{for } \arcsin \frac{\sigma_{t,\text{yield}}}{\sqrt{2\kappa_t a_I}} \leq \psi_G \leq \frac{\pi}{2}. \end{cases} \quad (4.2)$$

By comparing the expression of $\alpha(\llbracket u \rrbracket)$ in (4.2) with (2.9) and (2.10), and taking into account that $\alpha_{\text{ADHES}} = a_I$ is a constant, it is straightforward to extract a somewhat cumbersome expression of $\alpha_{\text{PLAST}}(\llbracket u \rrbracket)$ for $\arcsin \frac{\sigma_{t,\text{yield}}}{\sqrt{2\kappa_t a_I}} \leq \psi_G$, whereas $\alpha_{\text{PLAST}}(\llbracket u \rrbracket) = 0$ for $\psi_G \leq \arcsin \frac{\sigma_{t,\text{yield}}}{\sqrt{2\kappa_t a_I}}$. From (4.2) the maximum value of G_c is given by, cf. (3.9),

$$a_{II} = G_c(90^\circ) = a_I \left(1 + \frac{\kappa_t}{\kappa_H} \right) - \frac{\sigma_{t,\text{yield}}^2}{2\kappa_H}. \quad (4.3)$$

In the LEBIM, we will test the functional dependence defined in (4.2), governed by two parameters $\sigma_{t,\text{yield}}$ and κ_H , in addition to the parameters a_I , κ_n and κ_t of a basic linear elastic-brittle model which is (originally) insensitive to fracture mode mixity. Plots of the normalized fracture energy $G_c(\psi_G)/a_I$ in Fig. 3 qualitatively represent the behaviour observed in experiments [4, 5, 6, 8, 9].

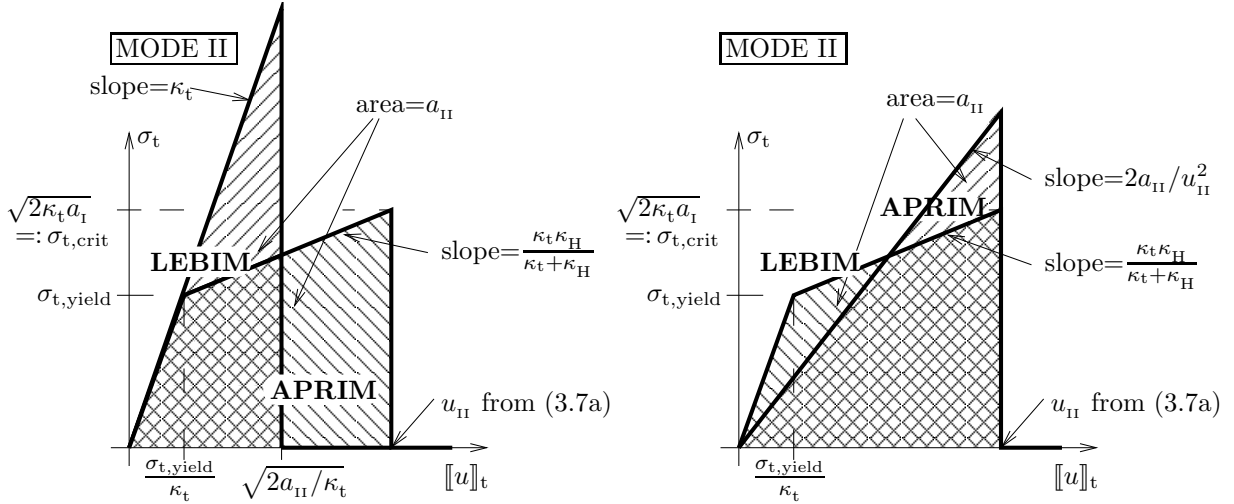


Fig. 2. Two scenarios for LEBIM in Mode II after fitting α by using APRIM with a specific \mathbb{A} . Left: $\mathbb{A} = \text{diag}(\kappa_n, \kappa_t)$. Right: $\mathbb{A} = \text{diag}(\kappa_n, 2a_{II}/u_{II}^2)$ with a_{II} and u_{II} from (3.7).

Let us remind that, as mentioned in Sect. 2, the above phenomenological relation (4.2), motivated by an elasto-plastic behaviour of an adhesive layer, can be rewritten in terms of ψ_u or ψ_σ instead of ψ_G . For an actual interface of some stiffness κ_t , the dependence of the fracture energy on the fracture-mode-mixity is controlled by two parameters: the yield stress $\sigma_{t,\text{yield}}$ and the hardening parameter κ_H . According to the plots presented in Fig. 3, the functional dependence of $\alpha(\psi_G)(= G_c(\psi_G))$ qualitatively represents the expected behaviour in view of the previous experimental results [4, 5, 6, 8, 9]. It can easily be observed from these plots that, as it was expected, $\sigma_{t,\text{yield}}$ has an influence on the threshold value of ψ_G for which $\alpha(\psi_G)$ changes its behaviour from a constant function to an increasing function,

while both $\sigma_{t,yield}$ and the hardening parameter κ_H control the value of ratio $\alpha(\psi_G)/a_I$, in particular its maximum value according to (4.3).

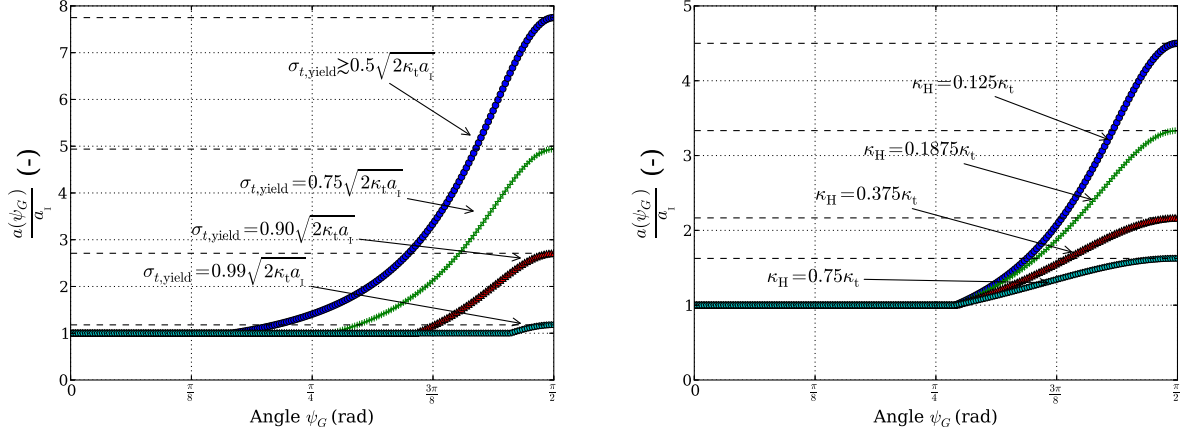


Fig. 3. Influence of $\sigma_{t,yield}$, considering $\kappa_H=0.11\kappa_t$ (left), and of κ_H , considering $\sigma_{t,yield}=0.75\sqrt{2\kappa_t a_I}$ (right), on the ratio $\alpha(\psi_G)/a_I$ given by (4.2). In both plots, the respective a_{II}/a_I value from (3.9) is plotted with the dashed line.

5. Illustrative 2D simulations and comparison

Single-domain example with LEBIM and APRIM comparison

A comparison of both models including varying fracture-mode-mixity of delamination is shown on a geometrically relatively simple but anyhow nontrivial two-dimensional example motivated by the pull-push shear experimental test used in engineering practice [27]. Intentionally, we use the same geometry, shown in Fig. 4, as in [20, 25] in order to have a comparison of our weak solution of the engineering non-associative visco-elastic model with a maximally-dissipative local solution of the associative inviscid model presented in [25]. In contrast to the previous sections, only one bulk domain is considered and Γ_C is a part of its boundary but this modification is straightforward; alternatively, one may also think about Ω_- as a completely rigid body in the previous setting.

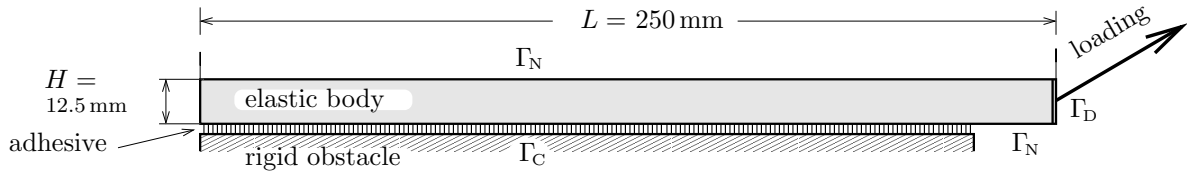


Fig. 4. Geometry and boundary conditions of the problem considered. The length of the initially glued part Γ_C is $0.9L = 225$ mm, the adhesive layer has zero thickness.

Here Ω_+ is a two-dimensional rectangular domain glued along the 90% of its bottom side Γ_C to a rigid obstacle, with the Dirichlet loading acting on the right-hand side Γ_D in the direction $(1, 0.6)$, see Fig. 4, increasing linearly in time with velocity 0.3 mm/s.

The bulk material is considered linear, homogeneous, and isotropic with Young's modulus $E = 70$ GPa and Poisson's ratio $\nu = 0.35$ (which corresponds to aluminum); thus $\mathbb{C}_{ijkl} = \frac{\nu E}{(1+\nu)(1-2\nu)}\delta_{ij}\delta_{kl} + \frac{E}{2(1+\nu)}(\delta_{ik}\delta_{jl} + \delta_{il}\delta_{jk})$ with δ_{ij} standing for the Kronecker symbol. In the LEBIM, the viscosity tensor $\mathbb{D} = \chi\mathbb{C}$ is considered with a relaxation time $\chi = 0.001$ s, which is very small in relation to the considered external-loading speed. Actually, we did not see any

essential difference for just merely elastic material with $\chi = 0$, although the inviscid variant of the LEBIM is not theoretically justified even as far as existence of solution concerns, and thus neither convergence of any numerical scheme.

For the adhesive, we took the normal stiffness $\kappa_n = 150$ GPa/m, the tangential stiffness with $\kappa_t = \kappa_n/2$, and the Mode-I fracture toughness $a_I = 187.5$ J/m². Furthermore, the engineering LEBIM was fitted to the APRIM using $\kappa_H = \kappa_t/9$ and $\sigma_{t,yield} \approx 0.79\sqrt{2\kappa_t a_I}$, which satisfies inequalities in eq. (3.8) and corresponds to a rather moderate mode-sensitivity $\alpha(90^\circ)/a_I \approx 4.36$.

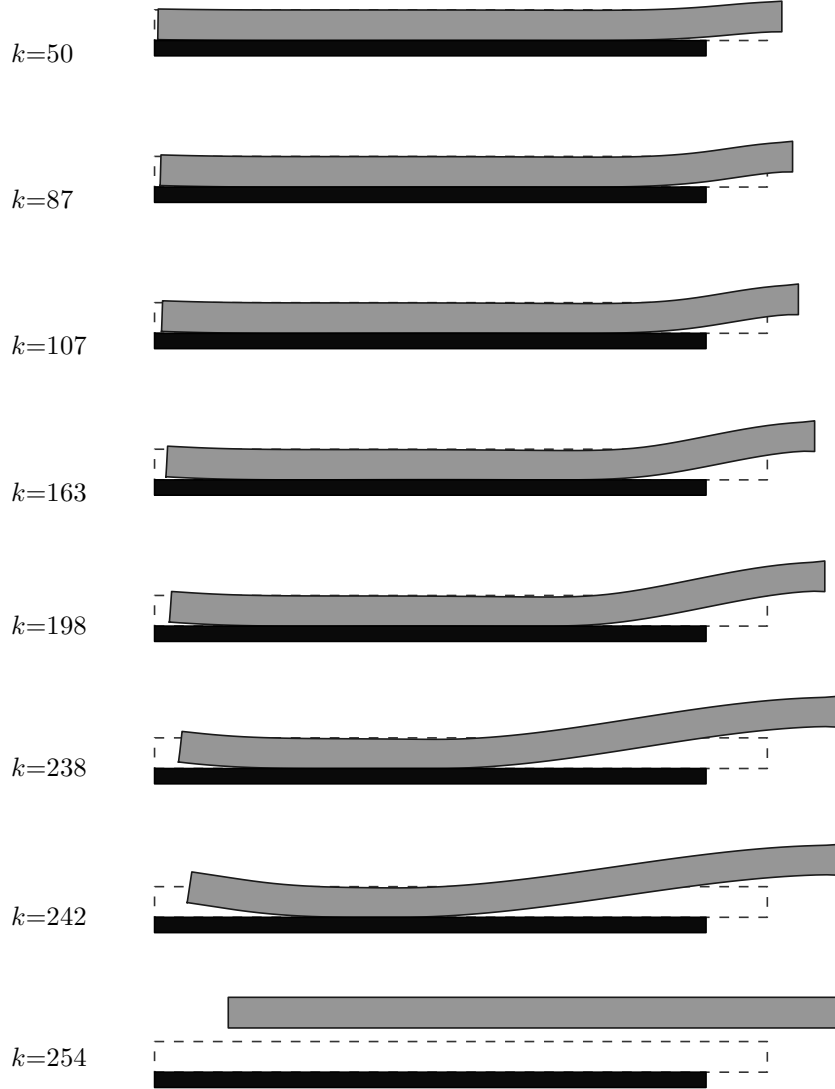


Fig. 5. Time evolution at eight snapshots of the deformed geometrical configuration (solid lines) compared with the original configuration (dashed lines) until complete delamination (displacement depicted magnified $100\times$). Calculations performed by the algorithm LEBIM.

This example exhibits remarkably varying mode of delamination. At the beginning, the delamination is performed by a mixed mode close to Mode I given essentially by the direction of the Dirichlet loading, see Figure 4, while later it turns rather to nearly pure Mode II. Yet, at the very end of the process, due to elastic bending the delamination starts performing also from the left-hand side of the bar opposite to the loading side, and thus again a mixed mode occurs. This relatively complicated mixed-mode behaviour is depicted as a “movie”

of 8 selected snapshots in Figure 5 calculated by the LEBIM fitted to the APRIM through the model of Fig. 2(Left), which would yield essentially similar picture.

The comparison of “global” quantities for the non-associative engineering LEBIM with $\alpha(\cdot)$ from the models of Fig. 2 with the associative (plasticity) APRIM is shown in Figures 6 and 7. As it can be observed the two models, even if they are based on similar assumptions and their parameters are fitted to provide similar responses, they show quite different behaviours. The observed differences can be explained by the fact that in APRIM the stiffness of the adhesive layer is progressively decreasing due to the presence of an interface plastic slip π , which may evolve at a portion of the interface before the damage suddenly occurs. Nevertheless, in LEBIM there is no variation of the adhesive layer stiffnesses before the damage occurs. In particular, this effect is clearly seen in Fig. 6, where the specimen stiffnesses begins to decrease with respect to that in LEBIM once the plastic slip begins to evolve. It worths mentioning that the LEBIM mode-mixity distribution is in a good agreement with the expected maximum a_{II}/a_I value.

Let us eventually briefly outline some implementation details for both models. We used the semi-implicit discretisation of the fractional-step type. Using an equidistant partition of the time interval $[0, T]$ with a time step $\tau > 0$, for LEBIM, the discrete variant of (2.6) looks as

$$\partial_u \mathcal{R}\left(\frac{u_\tau^k - u_\tau^{k-1}}{\tau}\right) + \partial_u \mathcal{E}(k\tau, u_\tau^k, z_\tau^{k-1}) \ni 0 \quad \text{and} \quad (5.1a)$$

$$\partial_z \mathcal{R}\left(u_\tau^k; \frac{z_\tau^k - z_\tau^{k-1}}{\tau}\right) + \partial_z \mathcal{E}(u_\tau^k, z_\tau^k) \ni 0, \quad (5.1b)$$

where u_τ^k denotes an approximation of $u(k\tau)$ and similarly for z_τ^k . This recursive scheme is to be solved for $k = 1, 2, \dots, T/\tau \in \mathbb{N}$. Note that both inclusions in (5.1) are decoupled from each other. For APRIM, the discrete variant of (3.5) looks as

$$\partial_u \mathcal{E}(k\tau, u_\tau^k, z_\tau^{k-1}, \pi_\tau^k) \ni 0, \quad \text{and} \quad \partial_\pi \mathcal{R}\left(\frac{\pi_\tau^k - \pi_\tau^{k-1}}{\tau}\right) + \partial_\pi \mathcal{E}(u_\tau^k, z_\tau^{k-1}, \pi_\tau^k) \ni 0, \quad \text{and} \quad (5.2a)$$

$$\partial_z \mathcal{R}\left(\frac{z_\tau^k - z_\tau^{k-1}}{\tau}\right) + \partial_z \mathcal{E}(u_\tau^k, z_\tau^k, \pi_\tau^k) \ni 0, \quad (5.2b)$$

Also this recursive scheme decouples (5.2a) from (5.2b).

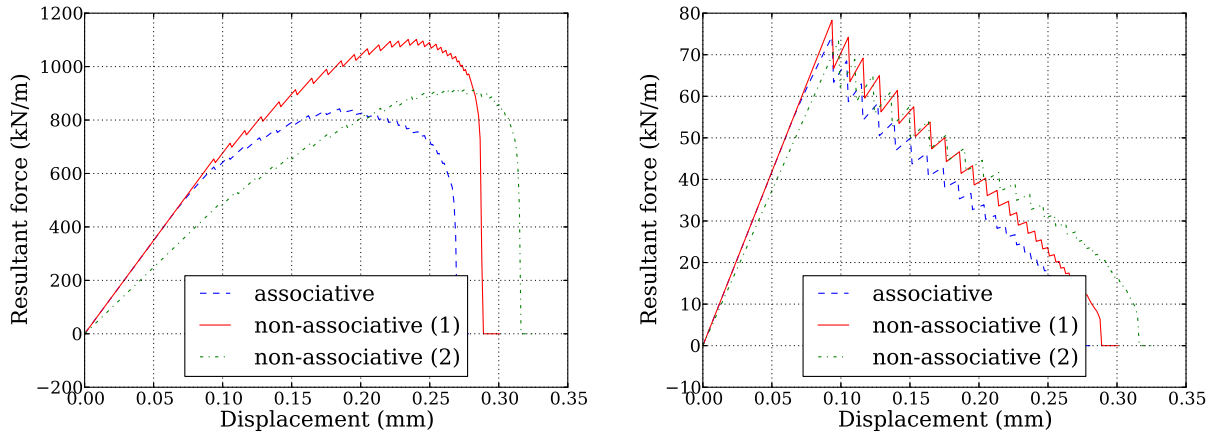


Fig. 6. The total force response evolving in time: the horizontal (left) and the vertical (right) components.

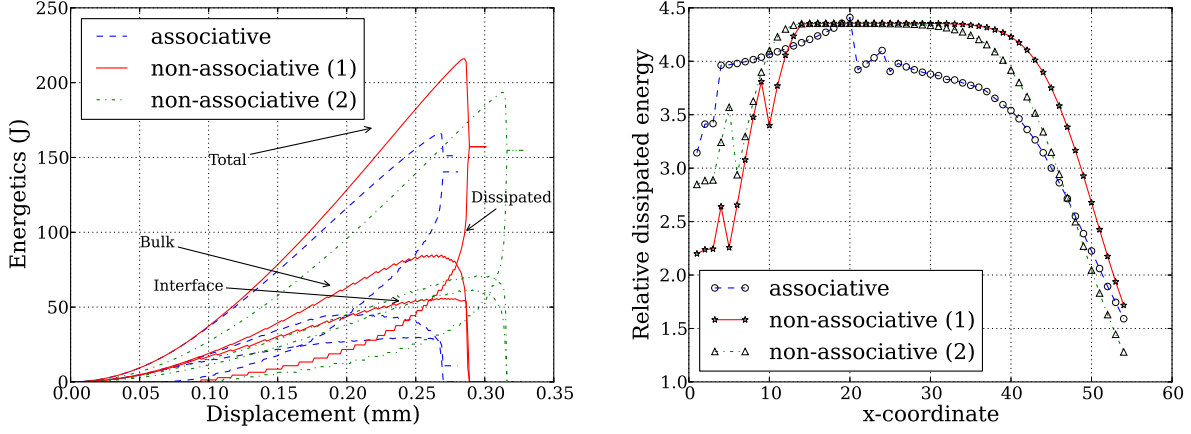


Fig. 7. **Left:** Time evolution of the energies: the bulk and the interfacial parts of the stored energy (together with the viscous contribution in the case of the LEBIM), the interfacial dissipated energy due to delamination, their sum = total energy. **Right:** Fracture-mode-mixity distribution along elements of Γ_C evaluated as the ratio of the overall dissipated energy to a_I after the delamination has been completed: value = 1 \sim Mode I, value = 4.36 = $a_{II}/a_I \sim$ Mode II.

For details of spatial discretisation by P1/P0-boundary-element method (P1 used for displacements, tractions and plastic slip π discretizations, whereas P0 used for the damage variable z discretization) and the outlined semi-implicit discretisation leading to a quadratic-programming or even a linear-programming problems, as well as of computer implementation in the case of both models LEBIM and APRIM, we refer to [18] and [20, 25], respectively. For BEM-implementation of the involved boundary-value problems see also [15, 23, 44, 45].

For the results presented in Figures 5–7, we have used 54 elements on Γ_C , i.e. $h = 4.1\bar{6}$ mm (=the size of a boundary segment in the present uniform discretization), and the time step $\tau = 5$ ms for both LEBIM and APRIM simulations.

Remark 5.1 (*Approximate maximum-dissipation principle*). We already mentioned at the end of Sect. 3 that (5.2) enjoys a guaranteed stability and convergence towards weak (called also local) solutions to the rate-independent problem (3.5). Yet, this class of solutions may be very wide if the stored-energy functional $\mathcal{E}(t, \cdot, \cdot, \cdot)$ is nonconvex, which is our case here, cf. [46] for a survey of variety of solution concepts, some of them may exhibit nonphysically early ruptures due to counting with a big energy cumulated in the elastic bulk or a nonphysical tendency of sliding to less dissipative Mode I even in situations where obviously Mode II should be preferred, cf. also [21]. It was discussed in [24] that the sound Hill’s maximum-dissipation principle [47] can serve as an additional attribute which may eliminate such unphysical weak solutions. In our case, it reads as

$$\int_{\Gamma_C} \xi(t) \dot{z}(t) \, dS = \max_{\tilde{\xi} \in K_z} \int_{\Gamma_C} \tilde{\xi} \dot{z}(t) \, dS \quad \text{and} \quad \int_{\Gamma_C} \zeta(t) \cdot \dot{\pi}(t) \, dS = \max_{\tilde{\zeta} \in K_\pi} \int_{\Gamma_C} \tilde{\zeta} \cdot \dot{\pi}(t) \, dS \quad (5.3)$$

for $t \in [0, T]$, where $\xi \in -\partial_z \mathcal{E}(u(t), z(t), \pi(t))$ and $\zeta \in -\partial_\pi \mathcal{E}(u(t), z(t), \pi(t))$ are available driving forces occurring already in (3.2) and $K_z := \partial_{\dot{z}} \mathcal{R}(0, 0)$ and $K_\pi := \partial_{\dot{\pi}} \mathcal{R}(0, 0)$ are the “elasticity domains” for the internal variable z and π , i.e. here

$$K_z = \{\xi \in L^1(\Gamma_C); \xi \geq -a_1 \text{ on } \Gamma_C\} \quad \text{and} \quad K_\pi = \{\zeta \in L^\infty(\Gamma_C; \mathbb{R}^{d-1}); |\zeta| \leq \sigma_{t, \text{yield}} \text{ on } \Gamma_C\}. \quad (5.4)$$

This principle holds rather automatically for a.a. (=almost all) time instants t for any weak solution to (3.2) which has \dot{z} and $\dot{\pi}$ absolutely continuous and then the integrals in (5.3) have the standard Lebesgue sense. On the other hand, during sudden ruptures where \dot{z} or $\dot{\pi}$ may concentrate in space and time to be only a general measure, the validity of (5.3) is not automatic and even analytically the integrals in (5.3) loses a sense even as dualities. It has been proposed in [24] to consider (5.3) rather integrated over the time interval $[0, T]$, which then reads, when also re-writing “max” over the elasticity domains in (5.3) equivalently as total variations, as

$$\int_{\Sigma_C} \xi(t) dz(t) dS = \int_{\Gamma_C} a_1(z(T) - z_0) dS \quad \text{and} \quad \int_{\Sigma_C} \zeta(t) \cdot d\pi(t) dS = \sigma_{t, \text{yield}} \int_{\Sigma_C} |\dot{\pi}(t)| dS dt \quad (5.5)$$

where the notations $\int \cdot dz(t)$ and $\int \cdot d\pi(t)$ stand for (lower) Pollard-Moore-Stieltjes integrals as used in [38], which are a Pollard-Moore modification of the so-called lower Riemann-Stieltjes integral, cf. e.g. [48], while the last integral is an integral of a total variation of the measure $\dot{\pi}$. Here, as suggested in [24], we apply (5.5) to the left-continuous piecewise-constant approximate solutions obtained by (5.2), let us denote them by \bar{u}_τ , \bar{z}_τ , and $\bar{\pi}_\tau$. Such a maximum dissipation principle for the approximate solution is expected to hold only approximately, if at all. The lower Pollard-Moore-Stieltjes integral can then be explicitly evaluated as well as the right-hand sides of (5.5), which yields

$$\int_{\Sigma_C} \bar{\xi}_\tau(t) d\bar{z}_\tau(t) dS = \sum_{k=1}^{T/\tau} \int_{\Gamma_C} \xi_\tau^{k-1} (z_\tau^k - z_\tau^{k-1}) dS \stackrel{?}{\sim} \int_{\Gamma_C} a_1(z_\tau^{T/\tau} - z_0) dS \quad \text{and} \quad (5.6a)$$

$$\begin{aligned} \int_{\Sigma_C} \bar{\zeta}_\tau(t) d\bar{\pi}_\tau(t) dS &= \sum_{k=1}^{T/\tau} \int_{\Gamma_C} \zeta_\tau^{k-1} (\pi_\tau^k - \pi_\tau^{k-1}) dS \stackrel{?}{\sim} \sigma_{t, \text{yield}} \sum_{k=1}^{T/\tau} \int_{\Gamma_C} |\pi_\tau^k - \pi_\tau^{k-1}| dS \\ &= \sigma_{t, \text{yield}} \int_{\Sigma_C} |\dot{\bar{\pi}}_\tau(t)| dS dt \end{aligned} \quad (5.6b)$$

where $\xi_\tau^k \in -\partial_z \mathcal{E}(u_\tau^k, z_\tau^{k-1}, \pi_\tau^k)$ and $\zeta_\tau^k \in -\partial_\pi \mathcal{E}(u_\tau^k, z_\tau^k, \pi_\tau^k)$, and where “ $\stackrel{?}{\sim}$ ” means that the equality holds at most only asymptotically for $\tau \rightarrow 0$ but even this is rather only desirable and not always valid. See [25, 21], for such sort of a-posteriori justification of the approximate local solution obtained by fractional-step discretisation as a stress-driven solution.

Multi-domain example with LEBIM model

The influence of the mixed-mode behavior, as well as, the efficiency of the LEBIM approximation, will be illustrated on an example of the Mixed-Mode Flexure (MMF) test [16, 19, 49] shown in Fig. 8. The specimen of the MMF test consists of two aluminium arms, bonded with a layer of resin adhesive. Detailed specimen dimensions and boundary conditions realizing the loading are shown in Figure 8; it should be noted the point support is on the borderline of compatibility (and, in fact, not compatible) with traces of H^1 -functions in dimension 2 but anyhow the numerical simulations did not see this slight discrepancy. The material properties of the bulk and interface are the same as in the previous example, however considering $\sigma_{t, \text{yield}} \approx 0.56\sqrt{2\kappa_t a_I}$ and inviscid conditions. Plane strain conditions

are considered for the problem, while a uniform mesh of 188 linear boundary elements is used to model the geometry. The evolution of the delamination of this double-stripe specimen is shown in Figure 9.

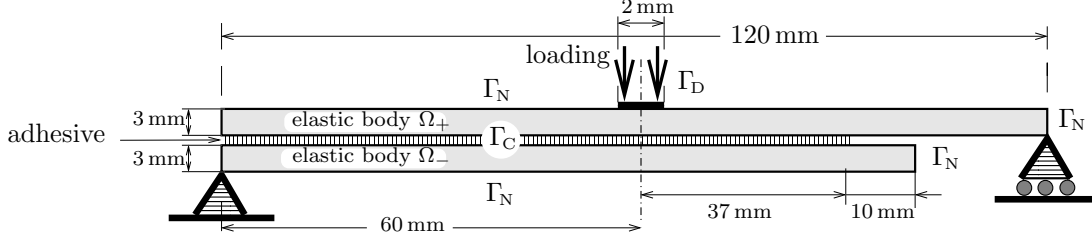


Fig. 8. Specimen configuration in the Mixed-Mode Flexure test.

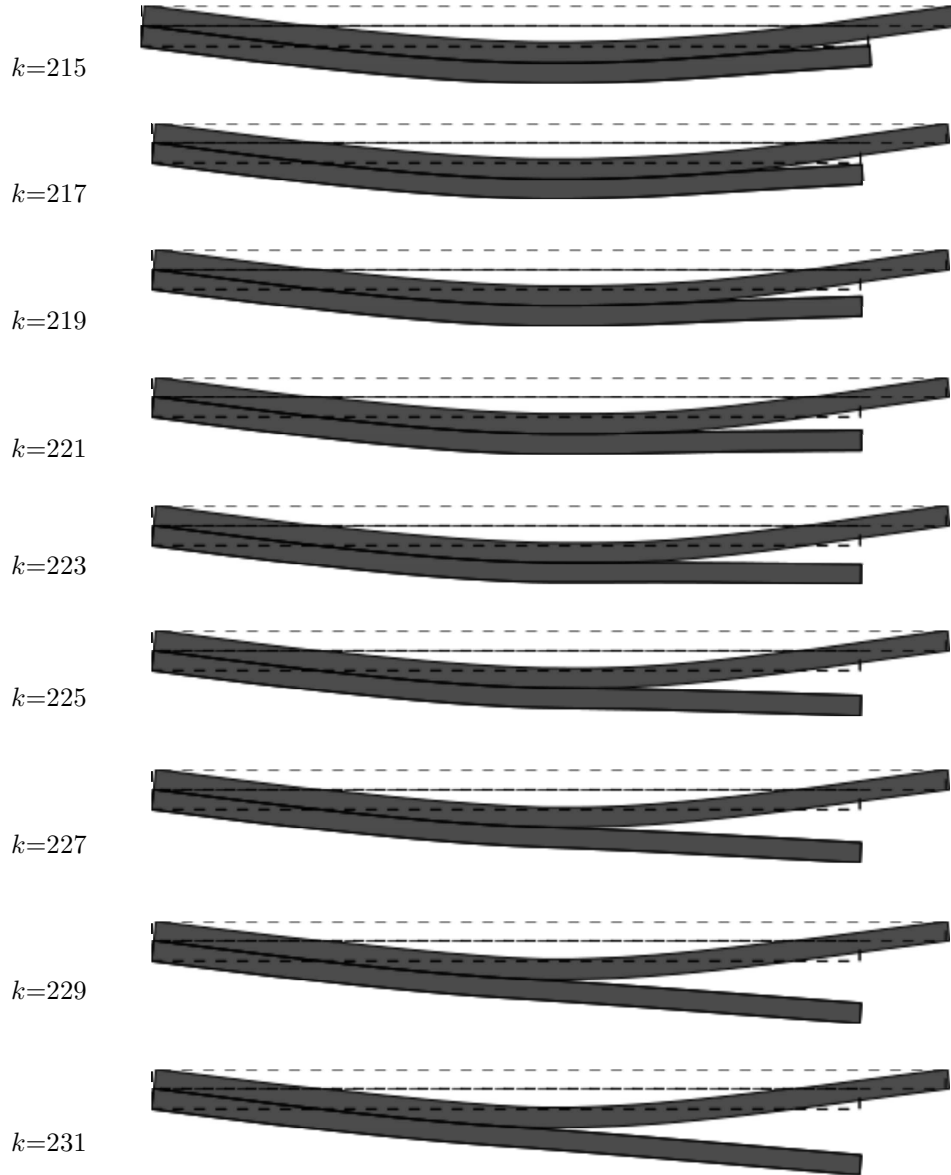


Fig. 9. Time evolution at ten snapshots of the deformed geometrical configuration (solid lines) compared with the original configuration (dashed lines, displacement depicted magnified $5 \times$). Calculations performed by the algorithm of LEBIM.

Finally, both scenarios for the LEBIM model shown in Fig. 2 are compared. The behaviour of their solutions is shown in Fig. 10, where the energetics of the delamination evolution are summarized (left) together with the load-deflection curves (right). Comparing

this behaviour with the former test from Fig. 5, whose results are depicted in Figs. 6 and 7, we can see that the scenario (1) yields again a bit earlier rupture than the scenario (2), as could be expected from the stress-relative displacements laws of these scenarios shown in Fig. 2. The length of the fractured part of the adhesive layer is the same in both scenarios, and the total dissipated energy is only slightly larger in the scenario (1) due to a slightly larger fracture mode mixity at the beginning of the crack propagation.

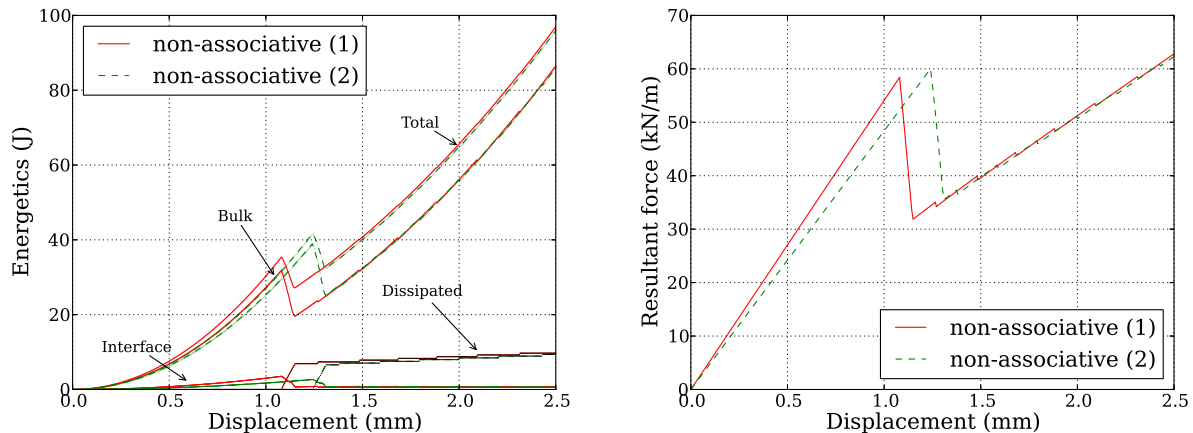


Fig. 10. Comparison of the evolution of energies (left) and load-deflection curves (right) for both scenarios of Fig. 2.

Acknowledgments

This research has been supported by the Spanish Ministry of Economy and Competitiveness and European Regional Development Fund (Project MAT2012-37387), the Junta de Andalucía and European Social Fund (Project of Excellence P08-TEP-04051), and from the Czech Science Foundation through the grants 201/10/0357, 201/12/0671, and 13-18652S, together with the institutional support RVO: 61388998 (ČR).

References

References

- [1] B. Halphen, Q. C. Nguyen, Sur les matériaux standards généralisés, *J. Méc.* 14 (1975) 39–63.
- [2] M. Frémond, Equilibre des structures qui adhèrent à leur support, *C.R. Académie des Sciences Paris* 295 (1982) 913–916.
- [3] M. Frémond, Equilibre des structures qui adhèrent à leur support, *J. Méc. Théor. Appl.* 6 (1987) 383–407.
- [4] L. Banks-Sills, D. Ashkenazi, A note on fracture criteria for interface fracture, *Int. J. Fract.* 103 (2000) 177–188.
- [5] J. W. Hutchinson, Z. Suo, Mixed mode cracking in layered materials, *Adv. Appl. Mech.* 29 (1992) 63–191.
- [6] K. M. Liechti, Y. S. Chai, Asymmetric shielding in interfacial fracture under in-plane shear, *J. Appl. Mech.* 59 (1992) 295–295.

- [7] V. Mantič, Discussion on the reference length and mode mixity for a bimaterial interface, *J. Eng. Mater. Technol.* 130 (2008) 045501–1–2.
- [8] J. G. Swadener, K. M. Liechti, A. L. deLozanne, The intrinsic toughness and adhesion mechanism of a glass/epoxy interface, *J. Mech. Phys. Solids* 47 (1999) 223–258.
- [9] A. G. Evans, M. Rühle, B. J. Dalgleish, P. G. Charalambides, The fracture energy of bimaterial interfaces, *Metall. Trans. A* 21A (1990) 2419–2429.
- [10] V. Tvergaard, J. W. Hutchinson, The influence of plasticity on mixed mode interface toughness, *J. Mech. Phys. Solids* 41 (1993) 1119–1135.
- [11] S. Bennati, M. Colleluori, D. Corigliano, P. S. Valvo, An enhanced beam-theory model of the asymmetric double cantilever beam (adcb) test for composite laminates, *Compos. Sci. Technol.* 69 (2009) 1735–1745.
- [12] P. Cornetti, V. Mantič, A. Carpinteri, Finite fracture mechanics at elastic interfaces, *Int. J. Solids Struct.* 49 (2012) 1022–1032.
- [13] V. Mantič, L. Távara, A. Blázquez, E. Graciani, F. París, A linear elastic-brittle interface model: application for the onset and propagation of a fibre-matrix interface crack under biaxial transverse loads, *Int. J. Fract.* 195 (2015) 15–38.
- [14] L. Távara, V. Mantič, E. Graciani, J. Cañas, F. París, Analysis of a crack in a thin adhesive layer between orthotropic materials: an application to composite interlaminar fracture toughness test, *CMES - Comput. Model. Eng. Sci.* 58 (2010) 247–270.
- [15] L. Távara, V. Mantič, E. Graciani, F. París, BEM analysis of crack onset and propagation along fiber-matrix interface under transverse tension using a linear elastic-brittle interface model, *Eng. Anal. Bound. Elem.* 35 (2011) 207–222.
- [16] N. Valoroso, L. Champaney, A damage-mechanics-based approach for modelling decohesion in adhesively bonded assemblies, *Eng. Fract. Mech.* 73 (2006) 2774–2801.
- [17] W. Han, B. D. Reddy, *Plasticity: Mathematical Theory and Numerical Analysis*, Springer-Verlag, New York, 1999.
- [18] M. Kružík, C. G. Panagiotopoulos, T. Roubíček, Quasistatic adhesive contact delaminating in mixed mode and its numerical treatment, *Math. Mech. Solids* 20 (2015) 582–599.
- [19] T. Roubíček, M. Kružík, J. Zeman, Delamination and adhesive contact models and their mathematical analysis and numerical treatment, in: V. Mantič (Ed.), *Math. Methods and Models in Composites*, Imperial College Press, 2014, Ch. 9, pp. 349–400.
- [20] T. Roubíček, V. Mantič, C. G. Panagiotopoulos, Quasistatic mixed-mode delamination model, *Discret. Contin. Dyn. Syst. - Ser. S* 6 (2013) 591–610.
- [21] R. Vodička, V. Mantič, T. Roubíček, Energetic versus maximally-dissipative local solutions of a quasi-static rate-independent mixed-mode delamination model, *Meccanica* 49 (2014) 2933–2963.
- [22] T. Roubíček, Adhesive contact of visco-elastic bodies and defect measures arising by vanishing viscosity, *SIAM J. Math. Anal.* 45 (2013) 101–126.
- [23] T. Roubíček, C. G. Panagiotopoulos, V. Mantič, Quasistatic adhesive contact of visco-elastic bodies and its numerical treatment for very small viscosity, *Zeitschrift angew. Math. Mech.* 93 (2013) 823–840.

- [24] T. Roubíček, Maximally-dissipative local solutions to rate-independent systems and application to damage and delamination problems, *Nonlinear Anal. Theory, Meth. Appl.* 113 (2015) 33–50.
- [25] T. Roubíček, C. G. Panagiotopoulos, V. Mantič, Local-solution approach to quasistatic rate-independent mixed-mode delamination, *Math. Models Meth. Appl. Sci.* 25 (2015) 1337–1364.
- [26] P. P. Camanho, C. G. Dávila, M. F. DeMoura, Numerical simulation of mixed-mode progressive delamination in composite materials, *J. Compos. Mater.* 37 (2003) 1415–1438.
- [27] P. Cornetti, A. Carpinteri, Modelling the FRP-concrete delamination by means of an exponential softening law, *Engr. Struct.* 33 (2011) 1988–2001.
- [28] R. Rossi, T. Roubíček, Adhesive contact delaminating at mixed mode, its thermodynamics and analysis, *Interfaces & Free Bound.* 14 (2013) 1–37.
- [29] R. A. Toupin, Elastic materials with couple stresses, *Archive Ration. Mech. Anal.* 11 (1962) 385–414.
- [30] R. Rossi, T. Roubíček, Thermodynamics and analysis of rate-independent adhesive contact at small strains, *Nonlinear Anal. Theory, Meth. Appl.* 74 (2011) 3159–3190.
- [31] M. Braccini, Interface adherence, in: M. Braccini, M. Dupeux (Eds.), *Mechanics of Solid Interface*, J. Wiley, 2012, Ch. 4, pp. 101–134.
- [32] A. A. Volinski, D. B. Bahr, M. D. Kriese, N. R. Moody, W. Gerberich, Nanoindentation methods in interfacial fracture testing, in: I. Milne, O. Ritchie, B. Karihaloo (Eds.), *Comprehensive Structural Integrity*, Elsevier, Amsterdam, 2003, Ch. 9, pp. 453–493.
- [33] M. Kolluri, M. H. L. Thissen, J. P. M. Hoefnagels, J. A. W. van Dommelen, M. G. D. Geers, In-situ characterization of interface delamination by a new miniature mixed mode bending setup, *Int. J. Fract.* 158 (2009) 183–195.
- [34] C. G. Panagiotopoulos, V. Mantič, T. Roubíček, BEM solution of delamination problems using an interface damage and plasticity model, *Comput. Mech.* 51 (2013) 505–521.
- [35] P. Podio-Guidugli, M. Vianello, Hypertractions and hyperstresses convey the same mechanical information, *Contin. Mech. Thermodyn.* 22 (2010) 163–176.
- [36] A. Mielke, F. Theil, On rate-independent hysteresis models, *Nonlinear Differ. Equ. Appl.* 11 (2004) 151–189.
- [37] A. Mielke, Differential, energetic and metric formulations for rate-independent processes, in: L. Ambrosio, G. Savaré (Eds.), *Nonlinear PDE's and Applications*, Springer, 2011, pp. 87–170.
- [38] A. Mielke, T. Roubíček, *Rate Independent Systems - Theory and Application*, Springer, New York, 2015.
- [39] S. Krenk, Energy release rate of symmetric adhesive joints, *Eng. Fract. Mech.* 43 (1992) 549–559.
- [40] S. Lenci, Analysis of a crack at a weak interface, *Int. J. Fract.* 108 (2001) 275–290.
- [41] K. Shahin, F. Taheri, The strain energy release rates in adhesively bonded balanced and unbalanced specimens and lap joints, *Int. J. Solids Struct.* 45 (2008) 6284–6300.

- [42] A. Carpinteri, P. Cornetti, N. Pugno, Edge debonding in FRP strengthened beams: Stress versus energy failure criteria, *Eng. Struct.* 31 (2009) 2436–2447.
- [43] R. Vodička, V. Mantič, An energetic approach to mixed mode delamination problem – an SGBEM implementation, in: V. Laš, R. Zemčík (Eds.), *Výpočty konstrukcí metodou konečných prvků*, University of West Bohemia, Plzeň, 2011, pp. 118–129, ISBN 978-80-261-0059-1.
- [44] S. Mukherjee, On boundary integral equations for cracked and for thin bodies, *Math. Mech. Solids* 6 (2001) 47–64.
- [45] F. París, J. Cañas, *Boundary Element Method, Fundamentals and Applications*, Oxford University Press, Oxford, 1997.
- [46] A. Mielke, Evolution in rate-independent systems, in: C. Dafermos, E. Feireisl (Eds.), *Handbook of Differential Equations, Evolutionary Equations*, 2, Elsevier, Amsterdam, 2005, pp. 461–559.
- [47] R. Hill, A variational principle of maximum plastic work in classical plasticity, *Q. J. Mech. Appl. Math.* 1 (1948) 18–28.
- [48] W. Rudin, *Principles of Mathematical Analysis*, 3rd Edition, McGraw-Hill, New York, 1976.
- [49] L. Távara, V. Mantič, A. Salvadori, L. J. Gray, F. París, Cohesive-zone-model formulation and implementation using the symmetric Galerkin boundary element method for homogeneous solids, *Comput. Mech.* 51 (2013) 535–551.